JOURNAL OF MATERIALS SCIENCE 15 (1980) 1978–1986

Pore formation during oxidative annealing of Al_2O_3- : Fe and slowing of grain growth by precipitates and pores

H. A. WANG, F. A. KRÖGER
Department of Materials Science, University of Southern California, Los Angeles, California 90007, USA

High-density samples of polycrystalline Al_2O_3 doped with iron retain their high density when annealed at high temperature in a reducing atmosphere, but pores are formed, both inside grains and at grain boundaries, and the density decreases upon annealing in oxidizing atmospheres. An explanation for these effects is proposed. The presence of pores and second-phase particles of $FeAl_2O_4$ is found to affect the physical properties and to slow grain growth. Grain size is proportional to the number of second-phase particles to the power $-\frac{1}{3}$ indicating that the number of second-phase particles per grain remains constant during grain growth.

1. Introduction

Annealing of low-density polycrystalline samples normally leads to a decrease in the porosity accompanied by an increase in the density. Annealing of high-density hot-pressed samples, on the other hand, has been reported to lead to a decrease in density by pore formation both for Al_2O_3 [1, 2] and Fe_2O_3 [3]. This effect was attributed to the liberation of gas adsorbed at grain surfaces, believed to be present even after hot-pressing *in vacuo* ([2] p. 42). The present paper describes density loss of Al_2O_3:Fe, prepared by hot-pressing *in vacuo*, upon annealing in an oxidizing but not in a reducing atmosphere. An explanation for this effect is proposed. The effect of the pores on grain growth and on the electrical conductivity is investigated.

2. Experimental procedure

Samples of polycrystalline α-Al_2O_3 doped with Fe were made from aluminium isopropoxide*, vacuum distilled at 150 to 160° C at a pressure of 10 to 15 mm Hg. An appropriate amount of $Fe_2(SO_4)_3 \cdot 10\,H_2O$ was dissolved in 2 litre deionized water. While stirring with a magnetic stirrer, pouring of 250 cm^3 purified aluminium isopropoxide into this solution led to the formation of a homogeneous gel. After drying and crushing, this material was decomposed overnight in a box furnace at 850° C. Hot-pressing of the oxide powder obtained was carried out in vacuum in a graphite die heated by r.f. power. In order to achieve approximately equal density (> 99.5% theoretical) and grain size (4 μm) for all samples, the conditions varied with the Fe content. For the samples doped with 0.05, 0.5 and 3 wt% Fe the time, temperature and stress of hot-pressing were respectively $\frac{1}{2}$ h, 1400° C, 4.1×10^7 Pa; $\frac{1}{2}$ h, 1450° C, 4.1×10^7 Pa and $\frac{3}{4}$ h, 1500° C, 4.8×10^7 Pa. Density was measured by the Archimedes method by weighing the samples in air and immersed in water.

The samples were annealed in a high-density alumina tube, closed at one end, heated in a Super Kanthal† furnace. Required oxygen partial pressures were maintained with the aid of commercial pure oxygen, air and CO/CO_2 mixtures.

A Cambridge S4-10 scanning electron microscope was used to study the morphology of the main phase, of second-phase particles (if any), and of pores. X-ray diffraction was used to determine the crystal structure of the second phase,

*Alfa Division, Ventron Corporation, Danvers, Massachusetts, USA.
†Kanthal Corporation, Wooster Street, Bethel, Conn.

 0022–2461/80/081978–09$02.90/0

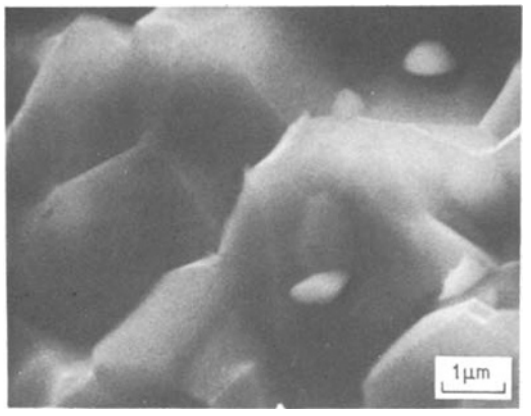

Figure 1 SEM of Al_2O_3–3 wt% Fe as-hot-pressed. The grain size is 4 μm, the second-phase particle size is 0.8 μm, × 8400.

and its composition was determined with the aid of an energy-dispersive X-ray unit* in the scanning electron microscope. Optical micrography of polished and etched samples was used to determine grain and pore size with the aid of the intercept method [4]. Polishing was performed with diamond paste of grain sizes ≈ 45, 20, 9, 6, 3 and 1 μm. Etching was done with boiling concentrated phosphoric acid for 2 to 3 min.

3. Results

Samples of Al_2O_3–3 wt% Fe, hot-pressed at 1500° C *in vacuo* under a pressure of 4.8×10^7 Pa, have a density corresponding to 99.9% theoretical density. The grain size is 4 μm while second-phase particles of 0.8 μm are present at grain boundaries and at triple junctions; they do not form a continuous film between the grains of the main phase (Fig. 1). The structure and density remain unchanged after annealing at 1600° C and $p_{O_2} = 10^{-6}$ Pa. X-ray analysis of the sample containing the second-phase particles using CuK_α radiation gives diffraction peaks at 31.16, 36.68, 59.00 and 64.83° in addition to those of α-Al_2O_3. These peaks, corresponding to interplanar distances of 2.87 Å (2 2 0), 2.45 Å (1 0 0), 2.30 Å (4 0 0), 1.56 Å (3 3 3) and 1.43 Å (4 . 4 0), identify the second phase as $FeAl_2O_4$.

Fig. 2a and b show the polished surface before and after etching of the sample doped with 3 wt% Fe annealed at 1600° C in $p_{O_2} = 10^{-6}$ Pa for 48 h. The shiny white area in the as-polished sample represents a second phase. After etching, the white area has disappeared and grain boundaries of Al_2O_3 show up. All second-phase particles are located at ternary points of grain boundaries.

Fig. 3 shows the grain size of the main phase and the second-phase particles as a function of time of annealing for Al_2O_3–3 wt% Fe annealed at 1600° C at $p_{O_2} = 10^{-6}$ Pa. The Al_2O_3 grains are equal-axis particles and grow according to a law, $d^n = d_0^n + kt$ with $n = 2$; the second phase follows a similar law with $n = 5$.

The grain size of Al_2O_3 and second-phase particles as a function of doping concentration for samples as-hot-pressed and after annealing for 16 h at 1600° C at $p_{O_2} = 10^{-6}$ Pa, is shown in Fig. 4. The second phase reduces grain growth at all concentrations, and the second-phase size increases with doping concentration.

Fig. 5 shows SEMs of samples after prolonged annealing at 1600° C with cyclic changing of oxygen pressure between 10^{-4} and 10^4 Pa, every 3 h.

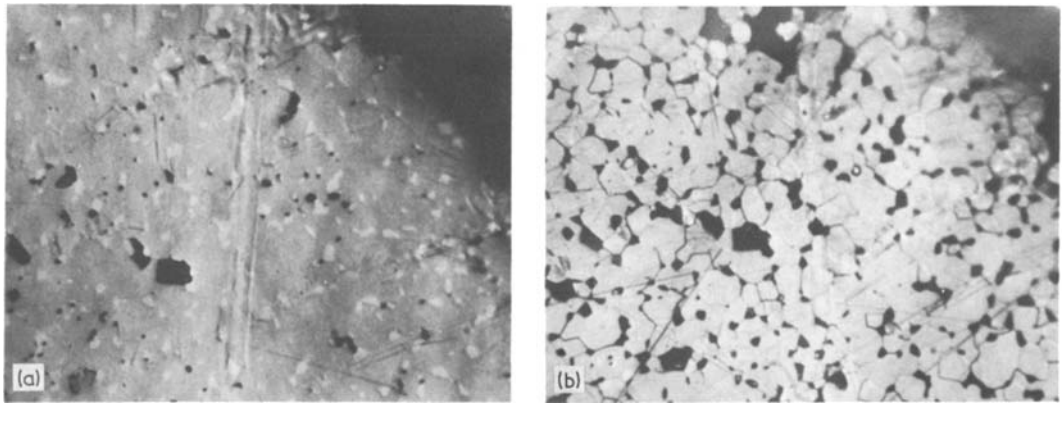

Figure 2 (a) Polished, (b) etched sample of Al_2O_3–3 wt% Fe annealed at 1600° C at $p_{O_2} = 10^{-6}$ Pa for 84 h, × 210.

*Tracer Northern, NS-880.

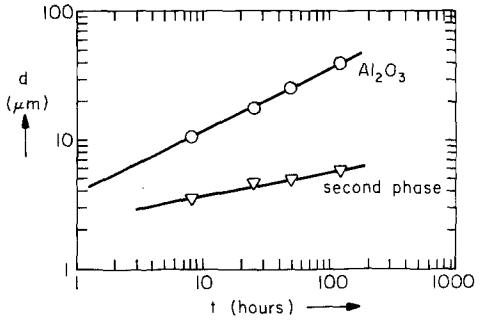

Figure 3 Logarithm of grain size (d) versus log t for Al_2O_3 – 3 wt% Fe annealed at 1600° C at $p_{O_2} = 10^{-6}$ Pa.

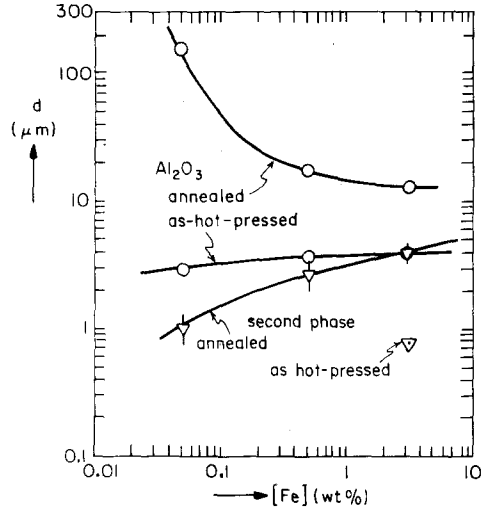

Figure 4 Grain size and second-phase particle size as a function of doping concentration for Fe-doped samples as-hot-pressed and after annealing at 1600° C at $p_{O_2} = 10^{-6}$ Pa for 16 h.

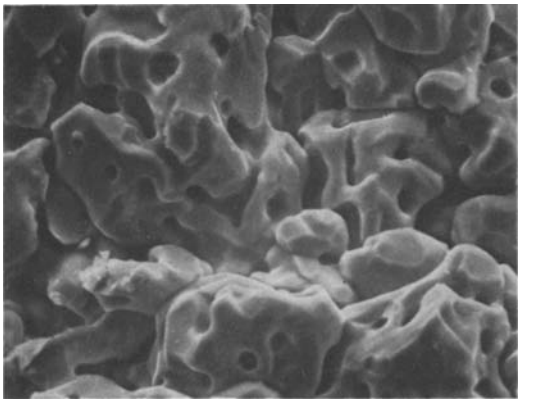

Figure 5 SEM of Al_2O_3 –3 wt% Fe annealed for 18 h at 1600° C in an atmosphere with cyclically changing oxygen pressure from 10^{-4} to 10^{4} Pa, × 840.

for 18 h. It is seen that a considerable number of pores have been formed. The majority of these pores are present at the grain boundaries, forming mostly an interconnected network, but some of the pores are formed inside the grains.

Table I shows the spectrographic analysis results of a sample Al_2O_3 –3 wt% Fe as-hot-pressed, the same sample after annealing at 1600° C in cyclically changed oxygen atmospheres for 18 h, and a slice of ~ 1 mm thick taken from the top of the alumina* tube which supported the latter sample during annealing.

After prolonged annealing, the concentration of all impurities except Si has been reduced. The iron concentration is decreased to about half of the as-hot-pressed value (3.0% to 1.4%). The end

TABLE I Wt % foreign elements in Al_2O_3 samples

Element	1	2	3	4	5	6	7
Ca	0.001 0	0.002 5	0.014	0.002 6	0.000 9	0.002 8	0.001 8
Cr	0.001 1	0.000 48	0.000 85	0.000 2	0.000 4	0.000 41	0.000 36
Cu	0.000 43	0.000 15	0.000 47	TR < 0.000 1	0.000 08	0.000 16	0.000 11
Fe	3.0	1.4	0.7	3.0	3.0	2.9	2.0
Mg	0.005 0	0.035	0.10	0.002 8	0.022	0.001 8	0.001 1
Mn	0.006 1	0.001 0	0.003 0	0.001 6	0.000 98	0.001 2	0.001 7
Mo	0.016	ND < 0.004	ND < 0.004	ND < 0.004	ND < 0.004	ND < 0.004	ND < 0.004
Ni	0.001 7	ND < 0.005	0.001 3	ND < 0.005	ND < 0.005	0.001 5	0.000 80
Si	0.018	0.039	0.33	0.022	0.019	0.009 4	0.011

(1) 3 wt% Fe, as-hot-pressed.
(2) 3 wt% Fe, after annealing at 1600° C with p_{O_2} cyclically changing between 10^{-4} and 10^{4} Pa every 3 h for 18 h.
(3) A slice 1 mm thick from the end of the AD-998 Alumina tube used to support sample 2 for annealing.
(4) 3 wt% Fe, after annealing at 1400° C in oxygen for 2 weeks.
(5) Sample 4, after another annealing treatment at 1400° C at $p_{O_2} = 10^{-6}$ Pa for 5 days.
(6) 3 wt% Fe, after annealing at 1550° C in powder of the same composition in oxygen for 18 h.
(7) Sample 6, after another annealing at 1550° C in powder of the same composition at $p_{O_2} = 10^{-6}$ Pa for 18 h.

*Coors AD-998 Al_2O_3 tube, reported to be 99.8% Al_2O_3, Coors Porcelain Co, Golden, Colorado, USA.

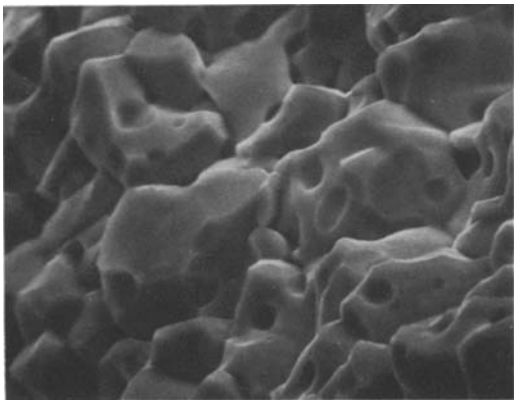

Figure 6 SEM of Al_2O_3–3 wt% Fe after annealing in oxygen at 1400° C for 14 days, × 1680.

of the supporting tube which was in contact with the sample reaches an iron content of 0.7%. Considering the volume of the coloured section of the Al_2O_3 tube, this accounts for all the Fe lost by the sample.

Samples annealed in oxidizing atmospheres invariably show pores, which do not disappear by a subsequent reducing treatment. This is true independence of whether the sample loses or does not lose iron. For example, a hot-pressed sample of Al_2O_3–3 wt% Fe, annealed for 2 weeks in 10^5 Pa oxygen at 1400° C, has a microstructure in which many pores have been formed (Fig. 6). The sample weight increases 0.53% by this annealing, which is close to the expected value calculated for the oxidation of the Fe^{2+} to Fe^{3+} for all the iron present. The sample density decreased from 99.8% to 97.5% theoretical value. Spectrographic analysis in Table I shows that there is no detectable iron loss. In the oxidized sample, no second phase is detected either by SEM or by X-ray diffraction. When the sample is annealed again at $p_{O_2} = 10^{-6}$ Pa at 1400° C for 5 days, the density is increased from 97.5% to 97.7% theoretical value, and the weight of the sample decreases by 0.55%, almost exactly the weight gain in the previous oxidation. Analysis again shows no detectable iron loss. Local composition analysis in the SEM shows that the second phase has again been formed.

The sample annealed for 48 h at 1600° C, $p_{O_2} = 10^{-6}$ Pa with the microstructure shown in Fig. 2a and b, was re-oxidized for 16 h in O_2 at 1600° C. Fig. 7a and b show the microstructure. Many pores are observed, most of them located at grain boundaries, but some of them found at the centre of grains.

In an effort to prevent the loss of iron at high temperature, a sample of Al_2O_3–3 wt% Fe was annealed at 1550° C in oxygen for 18 h, surrounded by powder of the same composition. Spectrographic analysis shows the iron loss is less than that of the unprotected sample (3.0% to 2.9% and 3.0% to 2.2%, respectively). The microstructure of this sample shows the presence of many pores in the centre of grains as well as at grain-boundary triple points. The size and amount of pores are only slightly smaller than those of the sample annealed in oxygen without powder protection. The density is decreased from 99.8% to 96.2% theoretical value.

Reduction for 18 h at 1550° C at $p_{O_2} = 10^{-6}$ Pa increases the density from 96.2% to 96.8%. The amount of pores is slightly smaller, but the pore size is increased. accompanied by an increase in grain size of the main phase and the reappearance of second-phase particles.

The formation of a second phase of $FeAl_2O_4$ in the reduced sample is in agreement with litera-

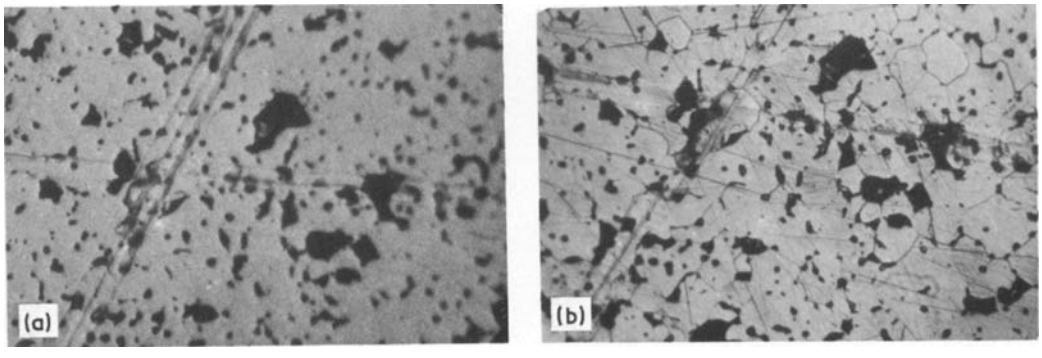

Figure 7 Optical micrographs of Al_2O_3–3 wt% Fe annealed at 1600° C at $p_{O_2} = 10^{-6}$ Pa for 48 h and in oxygen at 1600° C for 16 h (a) polished; (b) etched; × 180.

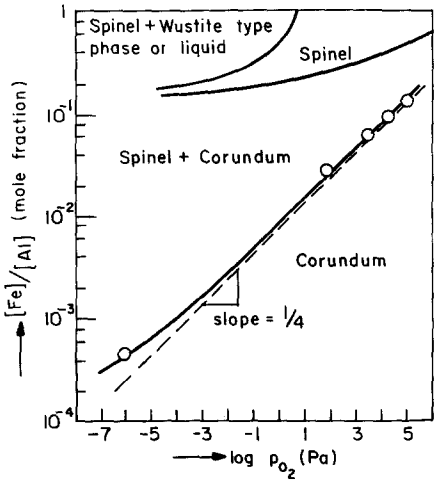

Figure 8 FeO–Al_2O_3–Fe_2O_3 phases as a function of p_{O_2} and Fe concentration at 1500° C.

ture data for the solubility of Fe in Al_2O_3 as $f(p_{O_2})$. Fig. 8 shows this solubility at 1500° C. obtained from data by Muan [5] and ourselves, combined with phase boundaries $FeAl_2O_4/Al_2O_3$ and $FeAl_2O_4/Fe_3O_4$ according to Roiter [6]. The solubility of $FeAl_2O_4$ in Al_2O_3 $\propto PO_2^{\frac{1}{4}}$ is expected on the basis of the incorporation reaction

$$2\,FeAl_2O_3 + \tfrac{1}{2}O_2 \rightarrow 2\,Fe_{Al}^{x} + 3\,O_O^{x} + 2\,Al_2O_3.$$

Fig. 9 shows grain size and pore size as functions of time for Al_2O_3–3 wt% Fe annealed in air at 1300, 1500 and 1600° C. The grains grow initially following the law, $d^n = d_0^n + kt$ with $n \approx 4$; pores follow the same law with $n \approx 3$. At longer times both grains and pores do no longer grow. The time needed to reach this stage decreases with increasing

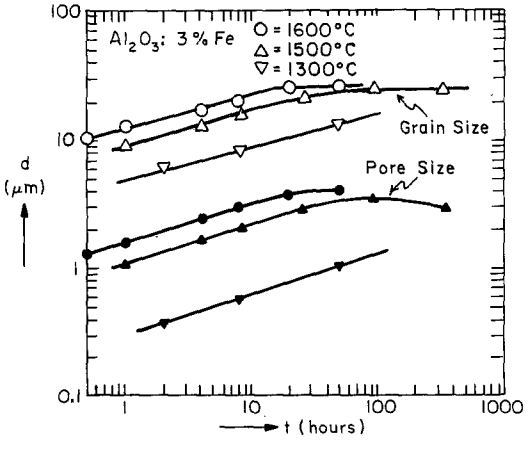

Figure 9 Grain size and pore size as a function of time for Al_2O_3–3 wt% Fe annealed in air at 1300, 1500 and 1600° C.

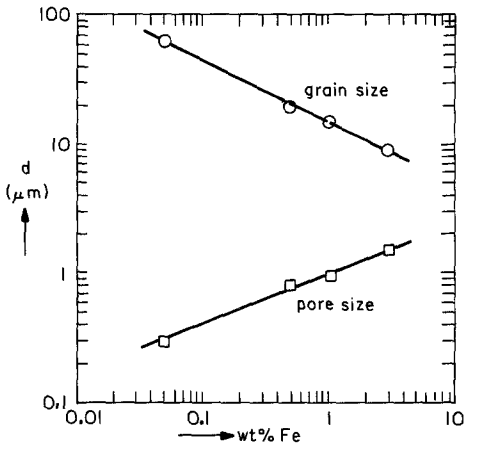

Figure 10 Grain size and pore size as a function of iron content after annealing for 1 h in air.

temperature, but the limiting grain and pore size is independent of temperature.

Fig. 10 shows grain size and pore size of Fe-doped samples annealed at 1500° C in air for 1 h as a function of doping concentration. The electrical conductivity at 1600° C as $f(p_{O_2})$ for samples Al_2O_3–3 wt% Fe of 4% and 16% porosity are shown in Fig. 11. Fig. 12a shows the emf, E, of oxygen concentration cells.

$$Pt,(p_{O_2})_I \mid \text{sample} \mid Pt,(p_{O_2})_{II}$$

with the samples of Fig. 11 as the electrolyte;

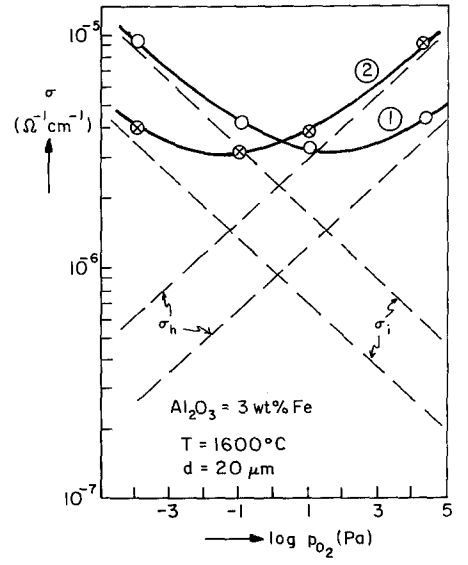

Figure 11 Electrical conductivity at 1600° C as a function of p_{O_2} for Al_2O_3–3 wt% Fe with (1) 4% porosity and (2) 16% porosity and partial ionic and electronic conductivities 6_i and 6_h.

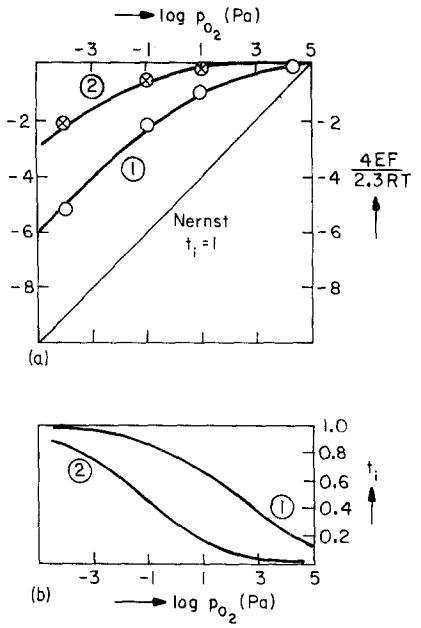

Figure 12 (a) EMF of an oxygen concentration cell based on samples (1) and (2) of Fig. 11. (b) Transference number $(t_i)p_{O_2,II}$ as a function of $(p_{O_2})_{II}$.

$(p_{O_2})_I = 1$ atm, $(p_{O_2})_{II}$ is variable. Fig. 12b shows the ionic transference number $(t_i)_{p_{O_2,II}}$ determined by differentiating the emf

$$(t_i)p_{O_2,II} = \frac{4F}{2.3RT}\left(\frac{\partial \log E}{\partial \log (p_{O_2})_{II}}\right)_{p_{O_2,I}}.$$

Values of the partial ionic and electronic (hole) conductivities $\sigma_i = \sigma t_i$ and $\sigma_h = \sigma(1-t_i)$ are shown in Fig. 11. The increase in porosity from 4 to 16% increases the hole conductivity by a factor 2.4 and decreases the ionic conductivity by a factor 2.5.

4. Discussion

4.1. Pore formation mechanisms

As shown in the experimental section, pore formation upon oxidative treatment may be, but need not be, accompanied by a loss of iron from the sample; pores are formed but no iron is lost if the annealing is performed at a relatively low temperature or if, at high temperature, loss of Fe is prevented by the presence of doped powder around the sample. Pores are formed and iron is lost upon annealing at high temperature without protection by powder.

After loss of iron, the lacking iron is found in the Al_2O_3 tube supporting the sample; it is probably the "sink" effect of the pure Al_2O_3 ceramics close to the doped Al_2O_3–Fe sample which is responsible for the loss, Fe migrating by surface diffusion to the absorbing ceramic tube. Movement of Fe inside the Al_2O_3 is fast [7, 8]. Since both Fe and O leave the sample, it is not surprising that pores are formed under these conditions.

More difficult is the explanation of pore formation – both inside the grains and at grain boundaries – in the absence of an Fe loss. In this case, pores may be formed by one or both of the following processes: (i) as a result of stress induced in the compact when the second phase is oxidized; (ii) by condensation of vacancies during climb of dislocations. Let us consider these processes separately.

(i) The solubility of Fe^{2+} in Al_2O_3 is limited, but that of Fe^{3+} is large. Oxidation changes the $FeAl_2O_4$ precipitate phase according to either

$$O_2 + 2FeAl_2O_4 \rightarrow Fe_2O_3 + 2Al_2O_3 \quad (1)$$

$$O_2 + 2FeAl_2O_4 \rightarrow Fe_2O_3 \cdot Al_2O_3 + Al_2O_3 \quad (2)$$

or

$$O_2 + 2FeAl_2O_4 \rightarrow (Fe_2O_3)_x \cdot (Al_2O_3)_{1-x} + (Al_2O_3)_{1+x} \cdot (Fe_2O_3)_{1-x}. \quad (3)$$

Of these three, Reaction 3 is the most likely process. After and during the completion of these reactions, Fe^{3+} will diffuse from the second-phase particles (where its concentration is high) into the neighbouring Al_2O_3 grains (where its concentration is relatively small) leading ultimately to a compact in which the iron is evenly distributed. Volume changes can have two origins. The first is a consequence of the fact that the volume per cation is different for $FeAl_2O_4 + Al_2O_3$ than for $(Al, Fe)_2O_3$. $FeAl_2O_4$ has a spinel structure with an effective volume per cation of $v_C = 22.25 \times 10^{-24}\,cm^3$. Al_2O_3 has an hcp (corundum) structure with $v_C = 21.22 \times 10^{-24}\,cm^3$. Fe_2O_3, also with a corundum structure, has $v_C = 25.3 \times 10^{-24}\,cm^3$.

Assuming Vegard's law to hold, a homogeneous solid solution Al_2O_3–3 wt% Fe_2O_3 (≈ 2 mol% Fe_2O_3) will have $v_C = 21.30 \times 10^{-24}\,cm^3$, and thus the change from Al_2O_3 (main phase) + $FeAl_2O_4$ (second phase) to homogeneous solid solution $(Al_{0.98}Fe_{0.02})_2O_3$ is accompanied by a volume effect of $-0.82 \times 10^{-24}\,cm^3$ per Fe atom or -3.9% of the second-phase volume, a direct reason for pore formation.

Additional reasons are found in the volume changes involved in the formation of the intermediate phases by Reactions 1 to 3.

Stoichiometric $Fe_2O_3 \cdot Al_2O_3$ has an orthorhombic structure with $v_C = 20.55 \times 10^{-24}$ cm^3. Non-stoichiometric $(Fe_2O_3)_{0.53}(Al_2O_3)_{0.47}$ has a different orthorhombic structure with $v_C = 24.67 \times 10^{-24}$ cm^3. Simple calculation shows that Reaction 1 is accompanied by a volume increase $\Delta v_C = 0.33 \times 10^{-24}$ cm^3 or 1.5% of the second-phase volume. Reactions 2 or 3 with stoichiometric or non-stoichiometric product phases, respectively, have $\Delta v_C = -1.5 \times 10^{-24}$ cm^3 or -6.5% of the second-phase volume, and $+1.27 \times 10^{-24}$ cm^3 or $+5.7\%$ of the second-phase volume. Thus the intermediate phases occupy either a larger or a smaller volume than the initial phases. In either case, part of these changes may remain in the sample and lead to pore formation. If the intermediate phase (present at triple grain boundaries) are larger, they exert a stress on the adjoining grains of Al_2O_3, pressing these apart, creating voids between grain surfaces. If the intermediate phases are smaller, homogenization may fill up part of the voids initially formed, but leaving some unfilled.

(ii) The second possible mechanism involved dislocations. The second-phase particles formed by Reactions 1 to 3 have either different lattice constants or different crystal structures than Al_2O_3, and dislocations must be present at the interfaces. As a result of the diffusion of Fe^{3+} into the Al_2O_3 grains (and Al^{3+} out of the grains), the mismatch decreases and the dislocations climb out of the mismatch zone [9]. This climb is accompanied by the creation of vacancies. Vacancies formed at the centre of the grains do not all diffuse to the grain boundary; the majority remain in the grains, where they precipitate, forming voids. In this way voids are formed in the centre of grains rather than at grain boundaries as for mechanism (i).

4.2. Influence of pores and second-phase particles on grain growth

Under the conditions to which Fig. 4 applies, all samples contain second-phase particles, and Fig. 4 shows that the presence of a second phase slows grain growth to an extent increasing with the amount (= total volume) of second phase.

However, it is clear that it is not the total volume of second phase that is important, but that the effect must be related to the way in which the second phase is distributed, i.e. to the size and number of second-phase particles. The number of second-phase particles per unit volume, C_{sp}, can be determined in two ways. In the first, the total volume of second phase per unit volume, V_{sp}, is determined from the difference Δx wt% of the iron content and the solubility ($\simeq 480$ ppm at 1600° C, $p_{O_2} = 10^{-6}$ Pa) using

$$V_{sp} = \frac{\Delta x}{100} \frac{\rho_{Al_2O_3}}{\rho_{FeAl_2O_4}} \frac{M_{FeAl_2O_4}}{M_{Fe}} \qquad (4)$$

with ρ the densities and M the molecular weights: $\rho_{Al_2O_3} = 3.97$, $\rho_{FeAl_2O_4} = 4.32$, $M_{FeAl_2O_4} = 174$ and $M_{Fe} = 55.85$. The values of V_{sp} so obtained are confirmed by measurement of the area fraction of the second phase in a photomicrograph which should be equal to the volume fraction [10]. With a volume per second-phase particle $v_{sp} \simeq d_{sp}^3$ (i.e. assuming a cube shape), and using d_{sp} determined from micrographs, $C_{sp} = V_{sp}/v_{sp}$ is found to be 7.0×10^8 and 1.4×10^9 cm^{-3} for the samples doped with 0.5 and 3 wt% Fe, respectively. The method cannot be applied to the low concentration sample. A second method determines the number from

$$C_{sp} = 2 p_1 p_s \qquad (5)$$

where p_1 is the number of precipitates intersected by a line of unit length and p_s the number of precipitates per unit area, both measured on a micrograph of known magnification. This method gives values of 2.8×10^5, 2.3×10^8 and 4.7×10^8 cm^{-3}, three times smaller than the values found by the other method.

Figure 13 shows growth rate constant, k, and average grain size, d, of the sample as a function of C_{sp} for samples with different doping concentration using for C_{sp} the values determined by method one, taking for the low concentration samples $C_{sp} = 8.4 \times 10^5$ $(= 3 \times 2.8 \times 10^5)$cm^{-3}. It is seen that k from the solution $d^n - d_0^n = kt$ is $k \propto C_{sp}^{-1/3}$ Thus d is a function of the number of second-phase particles rather than of their size or their total volume. With an average grain volume of $v_{gr} = \alpha d^3$ (with α intermediate between 1 and $\pi/6$, corresponding to cube-shaped and spherical grains), the number of second-phase particles per grain, $n_1 = C_{sp} V_{gr}$ is found to be $2.9\,\alpha$ for all samples. The number, n, of second phase particles adjacent to one grain is larger: if there are particles present at n_2 corners (shared by $\simeq 4$ grains) and at n_3 edges (shared by 3 grains), $n_1 = (n_2/4) + (n_3/3) \simeq (n/3.5)$. For a reasonable value $\alpha = 0.7$,

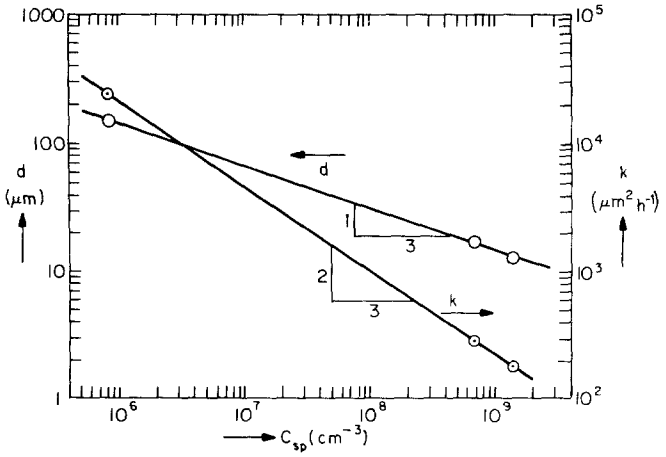

Figure 13 Rate constant k and grain size d of Al_2O_3–Fe annealed at 1600° C at $p_{O_2} = 10^{-6}$ Pa as a function of the concentration of $FeAl_2O_4$ precipitates; d is determined from a micrograph using $d = 1.5\ NM/L$, when L is the length of a straight line, N the number of grain boundary intersections, and M the magnification.

$n \simeq 7$, for steady-state morphology, in good agreement with the number found by inspection of photo micrographs (Fig. 14), which show precipitates at $\frac{1}{2}$ to $\frac{1}{3}$ of all corners ($\simeq 24$) [11] and at a few edges. Use of C_{sp} from Equation 5, would have given $n = 2.4$, not in agreement with observation.

The low value of n could be increased by changing the expression used to determine d from $d = 1.5\ NM/L$ to $d = 2\ NM/L$, but this would leave the discrepancy with C_{sp} as determined by method 1. It seems preferable to modify Equation 5 to

$$C_{sp} = 6 p_1 p_s \tag{6}$$

Since

$$n_1 = C_{sp} V_{gr},$$

$$d = \left(\frac{n_1}{\alpha}\right)^{1/3} C_{sp}^{-1/3} \tag{7}$$

in agreement with Fig. 13 if n_1/α is constant, as observed.

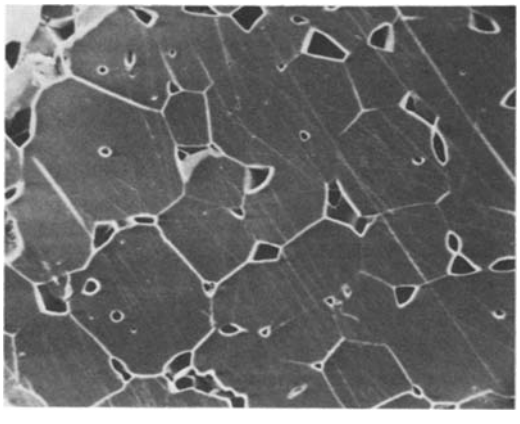

Figure 14 Photomicrograph of Al_2O_3 –3 wt% Fe, annealed at 1600° C, $p_{O_2} = 10^{-6}$ Pa, polished and etched. Pits indicate the position of second-phase particles removed by etching, × 840.

The growth law $d^n - d_0^n = kt$ with $n = 2$ observed in the present case where the grain growth is slowed in the presence of precipitates is not in agreement with that, with $n = 3$ expected for limitation by precipitates at corners [12–14]. The reason for this discrepancy is not clear.

The slowing effect of second-phase particles is not to be confused with the promoting effect of the dopant when dissolved in the grains at concentrations below the solubility limit, as observed for Fe by Rao and Cutler [15], for Mg and Ti by Harmer *et al.* [16] and for Mg by Johnson and Coble [17] and Peelen ([2] p. 20). The latter clearly demonstrated the transition between promotion and slowing of sintering as the solubility limit is reached.

From Fig. 10, it may be concluded that the size and amount of pores is proportional to the doping concentration. The pores slow grain growth, leading to a grain growth law, $d^n - d_0^n = kt$, with $n = 4$, corresponding to rate regulation by pore migration by volume diffusion [13]. After prolonged annealing, pores are interconnected to form a network, which practically stops the grain growth, causing the limited grain size displayed in Fig. 9.

The presence of pores also has a large influence on the mechanical properties. For example, at 1 to 2% porosity, the creep rate at 1400° C is about ten times higher than that of a comparable sample with 0.3% porosity. At even higher porosities (5 to 10%), the creep rate is extremely high and fracture occurs before a steady state is reached.

4.3. Influence of porosity on electrical conductivity

The increase of hole conduction and decrease of ionic conduction with increase in porosity is similar to the effect of grain boundaries on these

properties [18]. However, since we are dealing with polycrystalline samples, the effects observed must add to those of grain boundaries. The increase of hole conductivity must be attributed to a contribution of conduction via pore surfaces, which may be an order or so higher than that along grain boundaries or through the bulk. The decrease in ionic conduction indicates that pore surfaces just as grain boundaries have a low ionic conductivity, and pores as well as grain boundaries represent barriers for this type of conductivity, particularly pores cutting off conduction paths and decreasing the effective cross-section of the sample.

4.4. Pore formation during oxidation of superalloys (Ni, Cr, Al)

Oxidation of superalloys forms a surface film of Al_2O_3 containing up to 5 vol% pores close to the gas/oxide interface. These pores are believed to be formed by condensation of oxygen vacancies generated at the metal–oxide interface [19]. It is unlikely, however, that a porosity as large as 5% can be formed in this manner. It seems possible that the pores arise in the manner described in the present paper, with Ni instead of Fe.

References

1. R. W. RICE, "Fabrication and Characterization of Hot-Pressed Al_2O_3", Naval Research Laboratory, Washington, D.C., AD-709 556 (1970).
2. J. G. J. PEELEN, Thesis, Eindhoven University of Technology (1977).
3. A. G. CROUCH and R. T. PASCOE, *Proc. Brit. Ceram. Soc.* **20** (1972) 189.
4. M. I. MENDELSON, *J. Amer. Ceram. Soc.* **52** (1969) 443.
5. A. MUAN, *Amer. J. Sci.* **265** (1958) 413.
6. B. D. ROITER, *J. Amer. Ceram. Soc.* **47** (1964) 509.
7. D. V. IGNATOV, I. N. BELOKUROVA and I. N. BELYANIN, "Metallurgy and Metal Research" (All-Union Scientific and Technical Conference on the Use of Radioactive and Stable Isotopes and Radiation in the National Economy and in Science), Izv. Akad, Nauk, SSSR, Moscow, 1958) p. 326; NP-tr-448, p. 250 (1958).
8. V. I. IZEKOV and K. M. GORBUNOVA, *Fiz Met. Metallov.* 7 (1959) 713.
9. S. PRUSSIN, *J. Appl. Phys.* **32** (1961) 1876.
10. E. E. UNDERWOOD, A. R. COLCORD, and R. C. WAUGH, "Quantitive Relationships for Random Microstructures", Proceedings of the Third International Materials Symposium, "Ceramic Microstructures – Their Analysis, Significance, and Production: held at University of California, Berkeley, 13–16 June (1966), edited by R. M. Fulrath and J. A. Pask (Wiley, New York, 1968) p. 29.
11. C. S. SMITH, *Trans. AIME* **175** (1949) 15.
12. W. D. KINGERY and B. FRANCOIS, *J. Amer. Ceram. Soc.* **48** (1965) 546.
13. F. A. NICHOLLS, *J. Appl. Phys.* **37** (1960) 4599.
14. M. HILLERT, *Acta Met.* **13** (1965) 227.
15. W. R. RAO and I. B. CUTLER, *J. Amer. Ceram. Soc.* **56** (1973) 588.
16. M. HARMER, E. ROBERTS and R. J. BROOK, *Brit. Ceram. Soc. Trans.* **78** (1979) 22.
17. W. C. JOHNSON and R. L. COBLE, *J. Amer. Ceram. Soc.* **61** (1978) 110.
18. D. L. HOU, S. K. TIKU, H. A. WANG and F. A. KRÖGER, *J. Mater. Sci.* **14** (1979) 1877.
19. J. SMIALEK, private communication.

Received 9 October 1979 and accepted 8 January 1980.